

Resilient Preparation and Restoration Strategy for Integrated Electric-Gas Distribution Systems Considering Mobile Energy Storage

Han Wang, Cong Bai, *Graduate Student Member, IEEE*, Zhaoyu Wang, *Senior Member, IEEE*, Rajarshi Roychowdhury, *Senior Member, IEEE*

Abstract—Extreme events can interrupt both electricity and gas supply in an integrated electric-gas distribution system (IEGDS). This work proposes a two-stage resilient preparation and restoration strategy to efficiently restore both electric and gas load services in IEGDS after extreme events considering the utilization of mobile energy storage (MES). To minimize the load loss under the damage uncertainty and limited MES resources, a unified MES assigning and dispatching strategy is proposed to optimally coordinate the numbers and locations of pre-event and post-event MES dispatching. To address the MES assigning and pre-event dispatching problems under the damage uncertainty, a two-stage stochastic optimization model is developed, which is efficiently solved by a proposed selective progressive hedging (PH) algorithm. The out-of-sample analysis indicates that the proposed methods can achieve a 53.10% reduction in average load loss compared to scenarios without MES. In addition, the proposed unified MES assigning and dispatching strategy outperforms the preparation-only and restoration-only MES dispatching strategies by reducing 2.65% and 7.13% of average load loss, respectively. Moreover, the proposed selective algorithm can reduce 7.23% to 30.53% of the computational burden compared to the conventional PH algorithm.

Index Terms—IEGDS, MES, unified MES assigning and dispatching strategy, distributed solution method

I. INTRODUCTION

The secured and consistent energy supply through electricity and natural gas distribution networks is being threatened by increasingly frequent extreme events, leading to more and more concerns about the resilience of integrated electric-gas distribution systems (IEGDSs) [1]. In IEGDSs, the interdependence of electricity and gas supply networks significantly increases the operational complexity and makes the energy supply more vulnerable to damages, which introduces new challenges to ensuring the resilience of IEGDSs [2]–[4].

Considering the interdependence between electric and gas networks within IEGDSs, pioneering works have proposed efficient resilient operation strategies and models to mitigate the impacts of extreme events on IEGDS resilience [3]–[13]. In [5]–[7], optimal restoration strategies for IEGDS have been

developed by taking into account the coupling between power and gas networks through gas-fired distributed generators and gas compressors. Moreover, restoration strategies have been proposed to integrate the repair crew routing problem into the restoration process, enabling more efficient energy supply restoration in IEGDS [3], [8]–[10]. In addition, to handle the damage uncertainty after extreme events, robust and stochastic optimization models are developed in [12] and [13], respectively. By optimally operating and coordinating resilience resources, existing resilient operation strategies for IEGDS can realize highly efficient solutions as validated in the literature.

Meanwhile, with the advances in high-density and high-energy battery energy storage techniques, the application of utility-scale mobile energy storage (MES) has attracted additional attention [14]. Regarding distribution system resilience, MESs are recognized as spatially flexible energy resources that can be flexibly deployed to enhance system resilience [15]. In [15], [16], MESs are used together with other distributed energy resources in the distribution power system to enhance restoration performance. Some work [17], [18] also considered using MES to form microgrids within the distribution system and accelerate the restoration efficiency. Besides, the resilience enhancement-oriented MES investment strategy is also proposed in [19]. As demonstrated in prior studies [15]–[20], the application of MESs in distribution systems can significantly improve load restoration performances and mitigate the impacts of extreme events on distribution system resilience.

Motivated by antecedent works, this work proposes a resilient operation strategy for IEGDSs considering the utilization of MESs. The objective of the proposed strategy is to efficiently restore electric and gas loads by optimally utilizing and coordinating MESs with other resilience resources. In particular, although the majority of existing IEGDS resilient operation strategies focus on the post-event restoration stage, the pre-event preparation can also improve system preparedness against extreme events [21], [22]. In [23], [24], stochastic preparation strategies are proposed for distribution systems to develop preparation plans against extreme events. In addition to developing preparation plans, in [25], a two-stage pre- and post-disaster energy management model is developed to enhance the system preparedness against the tornado by increasing the energy stored in electric vehicles and natural gas storage. In [26], a multi-stage preparation and restoration model is proposed considering the spatiotemporal coupling

This work was partially supported by the U.S. Department of Energy Joint Office of Energy and Transportation under DE-EE0011234, the National Science Foundation under ECCS 2042314, and the Power System Engineering and Research Center (PSERC S-110). (*Corresponding Author: Zhaoyu Wang.*)

Han Wang, Cong Bai, and Zhaoyu Wang are with the Department of Electrical and Computer Engineering, Iowa State University, Ames, IA 50011 USA (e-mail: hanwang6@iastate.edu; congbai@iastate.edu; zwy@iastate.edu).

Rajarshi Roychowdhury is with the Grid Ops and Planning, Electric Power Research Institute (EPRI), Knoxville, TN 37932 USA (e-mail: rajarshirochowdhury@ieee.org).

relationship between different stages to assist DS operators in making resilient operation decisions against extreme events. Recognizing the significance of both pre-event preparation and post-event restoration, the proposed resilient operation strategy considers unifying both stages to minimize load loss.

In the proposed resilient operation strategy, efficient utilization of MESs is critical to the restoration performance. Because MESs are dispatched from the depot to desired locations through the transportation network (TN), the required transportation time of post-event dispatched MES could undermine the benefit of MESs and reduce the restoration efficiency, especially under degraded road conditions after extreme events. Pre-event dispatched MES can avoid such transportation time and start power injection immediately after the restoration begins. However, pre-event MES dispatching solutions may not be as accurate as post-event dispatching solutions due to the damage uncertainty. Hence, there is a trade-off between MES dispatching time and accuracy for both stages. To balance this trade-off, this work proposes a unified MES assigning and dispatching strategy considering the damage uncertainty and MES transportation time. In the proposed MES assigning and dispatching strategy, a portion of the MESs are assigned for pre-event dispatching to the most vulnerable parts of the system under the damage uncertainty. Then, after the damage information is revealed at the post-event stage, the rest MESs are accurately dispatched to assist in the system restoration.

In this context, how to make MES assigning and dispatching decisions under the damage uncertainty and limited MES resources is a key challenge for achieving efficient MES utilization and load restoration. To tackle this challenge, a two-stage stochastic mixed-integer programming problem is developed in this work. Because the formulated stochastic optimization model generates one set of operational variables and constraints for each scenario, the computational cost becomes extremely high as the simulated number of scenarios increases. To efficiently solve the formulated problem while ensuring the solution quality by considering a reasonable number of scenarios, a distributed solution method is devised based on the progressive hedging (PH) algorithm [27]. To accelerate the convergence of the developed distributed solution method, a selective PH algorithm is further proposed.

To distinguish the strategy proposed in this work from existing relevant studies, a comparative summary is presented in Table. I. As shown in the table, compared to existing works, this proposed innovative framework integrates pre-event preparation and post-event restoration problems to develop a unified resilient operation strategy for IEGDS considering the utilization of MES under damage uncertainties.

The key contributions of this work can be summarized as follows:

An integrated preparation and restoration strategy is proposed for IEGDSs to enable joint decision-making across stages considering the efficient utilization of MES under damage uncertainties. Moreover, a two-stage mixed-integer stochastic optimization model is formulated for making optimal preparation and restoration decisions.

TABLE I: Literature Comparison

Reference	Coupled Gas and Power Networks	Integrated Preparation and Restoration	Use of Mobile Energy Resource	Repair Crew Routing	Damage Uncertainty
[1]	✓	✗	✗	✗	✗
[5]–[7]	✓	✗	✗	✓	✗
[3]	✓	✗	✗	✓	✗
[8]–[10]	✓	✗	✗	✗	✓
[4], [12]	✓	✗	✗	✓	✓
[13]	✓	✗	✗	✓	✓
[15]	✗	✗	✓	✓	✗
[16], [17]	✗	✗	✓	✗	✗
[18], [28]	✗	✗	✓	✓	✓
[19], [29]	✗	✗	✓	✗	✓
[23], [24]	✗	✗	✗	✓	✓
[25]	✗	✓	✗	✗	✓
[26]	✗	✓	✓	✗	✗
Proposed	✓	✓	✓	✓	✓

A unified MES assigning and dispatching strategy is proposed to balance the trade-off between MES transportation time and dispatching accuracy under the damage uncertainty by enabling more flexible MES dispatching decision-making.

An efficient distributed solution method is developed based on the proposed selective PH algorithm to solve the formulated stochastic optimization model.

The rest of this paper is organized as follows: Section II describes the IEGDS resilient operation problem. Section III presents detailed problem formulations. The solution method is provided in Section IV. Section V gives experiment results and discussions. Section VI concludes this paper.

II. PROBLEM DESCRIPTION

This section provides an overview of the resilient operation problem for IEGDSs considering MES.

A. System Structure Overview

A representative structure of considered IEGDSs is shown in Fig.1. In the IEGDS, electricity and natural gas are distributed through the power distribution network (PDN) and the natural gas network (GN), respectively. The MES and repair crew are dispatched through the TN, in which the MESs and repair crew dispatching is modeled using travel time that depends on the mutual distance between two TN nodes.

In the GN, there is a gas well serving the gas loads and the fuel consumption of gas-fired distributed generators (DGs). It is assumed that the GN is radial so that the gas flow in all gas pipes is unidirectional. Gas pipes in the GN are classified as active and inactive pipes, depending on whether a gas pump is present, as shown in Fig. 1. In active pipes, the gas flow is driven by the gas pump operation that requires access to electricity. In inactive pipes, gas flows through the pipes due to nodal pressure differences. In the PDN, there are some gas-fired DGs in the network. Besides, the PDN also provides electricity to gas pumps in the GN.

In the IEGDS, the fuel consumption of gas-fired DGs in the PDN is modeled as gas demands in GN. Moreover, the gas pump energy consumption for driving gas flow in the GN is modeled as electricity demands in the PDN. Hence, the PDN and GN in this work are coupled through the gas-fired DGs and gas pumps, as indicated by the dashed arrows in Fig. 1.

In this work, the proposed resilient operation strategy aims to minimize the total load loss in the PDN and GN after extreme events by optimally operating and coordinating the resilient resources including tie-lines, repair crew, gas-fired DGs, and MES. As both pre-event preparation and post-event restoration are important for minimizing load loss, both stages are considered in the proposed resilient operation strategy.

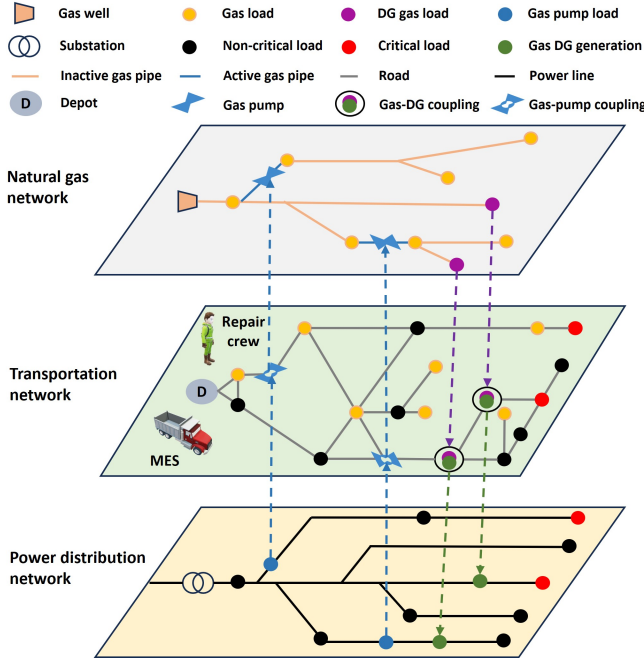


Fig. 1: System structure overview

B. Pre-Event Preparation

In the pre-event stage, flexible resources should be optimally dispatched to maximize the load restoration efficiency. In this work, MESs are considered flexible resources that can be dispatched to PDN nodes at the pre-event stage to facilitate efficient restoration actions after the extreme event.

At this stage, the damage information is unknown, and extreme event predictions should be made to generate fault scenarios based on the fragility model of the system [23], [24]. Besides, since natural gas pipes are usually buried underground [30], it is assumed that the gas pipes in the GN will not be damaged, and faults can only occur in the PDN. Based on the fault scenarios, optimal restoration can be performed by utilizing and coordinating MES with other resilience resources. In this work, multiple fault scenarios are generated at the pre-event stage to ensure the solution quality. Because the optimal MES dispatching solution is fault scenario dependent, the MES dispatching at the pre-event preparation stage should consider coordinating the MES dispatching solutions of different fault scenarios. The coordinated MES dispatching result may not be consistent with the optimal MES dispatching solutions for individual fault scenarios. Hence, the pre-event MES dispatching solution suffers from the accuracy problem.

C. Post-Event Restoration

At the post-event stage, the damage information becomes known parameters and the restoration problem aims to mini-

mize the total load loss in the PDN and GN. The restoration process includes PDN reconfiguration, dispatching the repair crew to fix damaged components, scheduling DGs and MES to provide operational support for serving the loads, and scheduling gas pumps to drive gas flows in the GN.

In the restoration process, it is assumed that DGs and tie-lines can be remotely controlled. Besides, the repair crew and MES are dispatched from the depot to the desired locations to fix damaged components and provide grid support, respectively. At the post-event stage, since the damage information is revealed, the MESs can be accurately dispatched to provide the most efficient grid support and minimize load loss. However, accurately dispatching MES after damage information is revealed requires transportation time, especially under degraded road conditions after extreme events. The transportation time can reduce the benefit of MES because MES cannot immediately inject power into the PDN as the restoration begins. Hence, the post-event MES dispatching solution faces the transportation time problem.

D. Unified MES Assigning and Dispatching Strategy

As a key resilience resource in this work, the efficient utilization of MES is critical to restoration efficiency. As discussed, the pre-event MES dispatching is less accurate than the post-event MES dispatching, but the post-event MES dispatching costs additional transportation time compared to pre-event MES dispatching. To balance the trade-off between MES transportation time and dispatching accuracy, this work proposes a unified MES assigning and dispatching strategy. The proposed strategy not only optimizes the MES dispatching locations in both the preparation and restoration stages but also coordinates the number of MES being dispatched in each phase. Hence, the proposed strategy unifies the MES assigning and dispatching problems to coordinate the pre-event and post-event MES dispatching solutions. The optimal MES assigning and dispatching solutions is achieved by solving both the pre-event preparation and the post-event restoration problems.

At the pre-event stage, the optimal preparation problem identifies the most favorable MES dispatching locations that would minimize the expected load loss considering all the generated fault scenarios and their probabilities. In addition to MES dispatching locations, determining the number of MES to be dispatched at the pre-event stage and the number of MES reserved for more accurate post-event dispatching is also important because the total number of MES is limited. Hence, the preparation problem also needs to optimally combine the pre-event and post-event MES dispatching solutions to determine the optimal number of MES being dispatched in each stage. By solving the optimal preparation problem, the MES assigning problem is addressed, and the optimal pre-event MES dispatching solution is also obtained.

Notably, only the pre-event MES dispatching solution is implemented by solving the pre-event preparation problem. Although a restoration problem is solved and a post-event MES dispatching solution can be obtained for each fault scenario generated in the preparation stage, the post-event MES dispatching decisions obtained for different fault scenarios in the preparation problem may or may not be implemented.

At the post-event stage, the damage information is revealed, and part of the MESs are already dispatched at the pre-event stage. The post-event restoration problem optimally dispatches the rest MESs and coordinates all resilient resources to minimize the load loss based on the damage information and pre-event MES dispatching results. By solving the post-event restoration problem with actual damage information, the post-event MES dispatching problem in the proposed strategy is also addressed.

III. PROBLEM FORMULATION

This section first presents the formulation of the two-stage stochastic mixed-integer preparation problem, then gives the deterministic post-event restoration problem formulation.

A. Pre-Event Optimal Preparation

To handle damage uncertainties following extreme events, an efficient approach is to model uncertain damages using representative fault scenarios generated from power system fragility models [23], [24]. Using the generated representative fault scenarios and corresponding probabilities, a two-stage stochastic optimization model is formulated to minimize the expected load loss against damage uncertainty. In the pre-event stage, the two-stage stochastic preparation problem optimizes the operation of resilience resources, especially the combination of pre-event and post-event MES dispatching solutions, to minimize the expected load loss considering all the generated fault scenarios $s \in S$.

$$\min_{\substack{X_j, Y_{s,j}; U_{s,j,t}; Z_{s,t}^e, Z_{s,t}^g; R_s \\ s \in S}} \sum_{t \in T} \sum_{j \in J} W_j^e P_{s,j;t}^{loss} + \sum_{t \in T} \sum_{m \in M} W^g G_{s,m;t}^{loss} + \sum_{t \in T} \sum_{d \in D} W^{ft} FT_{s;d} \quad (1)$$

In the objective function, the first-stage decision variables are pre-event MES dispatching decisions X_j . For each PDN node j , a binary variable X_j is used to indicate if an MES is dispatched to node j at the pre-event stage, and $X_j = 1$ means that an MES is dispatched to PDN node j at the pre-event stage. The second-stage decision variables are scenario-dependent variables, which include the post-event MES dispatching decisions $Y_{s,j}$, the MES availability indicator $U_{s,j,t}$, the power system operation decisions $Z_{s,t}^e$, the gas system operation decisions $Z_{s,t}^g$, and repair crew dispatching decisions R_s for each damage scenario s . In the second stage, the binary post-event MES dispatching decision $Y_{s,j} = 1$ means that an MES is dispatched to node j at the post-event stage of scenario s . Due to the limitation of MES transportation time, the availability of pre-event and post-event dispatched MES is different. To address this issue, an auxiliary variable $U_{s,j,t}$, which depends on both the pre-event and post-event MES dispatching decisions, is introduced to indicate when MES is available at node j in scenario s . The second-stage PDN operation variables $Z_{s,t}^e$ include the activation status of PDN nodes, switching of distribution lines, gas-fired DG generation, MES discharging, and gas pump operation. The second-stage GN operation variables $Z_{s,t}^g$ include gas procurement, gas consumption, DG gas fuel supply, gas network nodal pressure, and gas flow in gas pipelines. The repair crew dispatching

decision variables R_s include the crew routing decisions and fault repair times.

The probability of each generated fault scenario s is denoted by p_s . For each PDN node $j \in J$, the electric load loss in scenario s at time t is given by $P_{s,j;t}^{loss}$. Similarly, for each GN node $m \in M$, the gas load loss in scenario s at time t is given by $G_{s,m;t}^{loss}$. For the restoration process, the optimization horizon is given by T , and the problem optimization resolution is given by Δt . The weights for electric loads and gas loads are given by W_j^e and W^g , respectively. There are critical and non-critical electric loads, but gas demands are considered equally important. The fixing time of each damaged component $d \in D$ in scenario s is denoted by $FT_{s;d}$, and the weight for fixing the damaged components is given by W^{ft} .

The first and second terms in the objective function represent the load loss in the PDN and GN, respectively. The third term is added to ensure that all the damaged components will be fixed as soon as possible. Notably, to ensure that minimizing the fixing time will not reduce load restoration efficiency, the weight W^{ft} should take a small enough value compared to the weights of electric and gas load loss.

1) Power System Constraints

The PDN nodal power balance constraints are as follows:

$$P_{s,j;t}^{dg} + \sum_{i \in I'(j)} P_{s,ij;t} + \sum_{m \in M} P_{s,j;t}^m = \sum_{i \in I(j)} P_{s,j;t}^l + \sum_{s,j,t} P_{s,j;t}^{gp} + \sum_{i \in I(j)} P_{s,ji;t} \quad (2)$$

$$Q_{s,j;t}^{dg} + \sum_{i \in I'(j)} Q_{s,ij;t} + \sum_{m \in M} Q_{s,j;t}^m = \sum_{i \in I(j)} Q_{s,j;t}^l + \sum_{s,j,t} Q_{s,j;t}^{gp} + \sum_{i \in I(j)} Q_{s,ji;t} \quad (3)$$

$$P_{s,j;t}^l = u_{s,j,t} P_{j;t}^l \quad (4)$$

$$P_{s,j;t}^{loss} = P_{j;t}^l - P_{s,j;t}^l \quad (5)$$

The real and reactive power generations of gas-fired DGs are represented by $P_{s,j;t}^{dg}$ and $Q_{s,j;t}^{dg}$, respectively. The real and reactive power flow from node i to j are denoted by $P_{s,ij;t}$ and $Q_{s,ij;t}$, respectively. Sets $I'(j)$ and $I(j)$ denote the parent nodes and child nodes of node j , respectively. The electric load is given by $P_{s,j;t}^l$ and $Q_{s,j;t}^l$, and the real and reactive MES power injections are denoted by $P_{s,j;t}^m$ and $Q_{s,j;t}^m$. The real and reactive gas pump power are given by $P_{s,j;t}^{gp}$ and $Q_{s,j;t}^{gp}$, respectively. The load for node j at time t without interruption is denoted by $P_{j;t}^l$, which is an input value in the problem. The binary variable $u_{s,j,t}$ represents the energization status of node j at time t in scenario s . Constraints (2) and (3) are the real and reactive nodal power balance constraints for PDN nodes, respectively. Notably, demand response is not available in this work. Hence, the load of node j at time t in scenario s is only dependent on its energization status $u_{s,j,t}$ and the uninterrupted load $P_{j;t}^l$, as shown in constraint (4). The electric load loss is calculated using 5.

The power flow constraints [31] are as follows:

$$V_{s;i;t} - V_{s;j;t} - 2(r_{ij}P_{s;ij;t} + x_{ij}Q_{s;ij;t}) + M(1 - a_{s;ij;t}) \leq 0 \quad (6)$$

$$V_{s;i;t} - V_{s;j;t} - 2(r_{ij}P_{s;ij;t} + x_{ij}Q_{s;ij;t}) - M(1 - a_{s;ij;t}) \leq 0 \quad (7)$$

$$V_{min}U_{s;j;t} \leq V_{s;j;t} \leq V_{max}U_{s;j;t} \quad (8)$$

$$V_{s;1;t} = 1 \quad (9)$$

The resistance and reactance of power distribution lines are denoted by r_{ij} and x_{ij} , respectively. $V_{s;j;t}$ is the square of nodal voltage. The binary variable $a_{s;ij;t}$ denotes the connection status of line ij , and $a_{s;ij;t} = 1$ means that line ij is connected. M is a large enough constant. The square of lower and upper voltage limits are denoted by V_{min} and V_{max} , respectively. Constraints (6) and (7) describe the voltage difference between two end nodes of each connected line. Constraint (8) ensures that the nodal voltages of energized nodes are within the safe range. Constraint (9) ensures that the substation always maintains its voltage at 1 p.u.

Notably, unbalanced power flow is not considered in this work. If the three-phase unbalanced power flow needs to be accommodated, the power flow constraints (6) and (7) should be modified. Specifically, when calculating the voltage differences between connected nodes, the line impedance would need to be replaced with the (3 × 3) impedance matrix of the branches [32]. In addition, if three-phase synchronous generators are involved, generator current unbalanced factors need to be constrained to prevent generator tripping [33].

Because operating tie-lines can change the topology of the PDN, the radiality constraints [34] are needed to ensure the radial PDN topology during the reconfiguration process.

$$b_{s;ij;t} + b_{s;ji;t} = a_{s;ij;t}; \delta_{ij} \in E \quad (10)$$

$$b_{s;ij;t} = 0; \delta_{ij} \in R \quad (11)$$

$$\sum_{i:j \in E} b_{s;ji;t} = \sum_{j \in R} u_{s;j;t}; \delta_j \in J \cap R \quad (12)$$

$$\sum_j P_{s;ij;t} - \sum_j a_{s;ij;t}M; \delta_{ij} \in E \quad (13)$$

The auxiliary variables $b_{s;ij;t}$ and $b_{s;ji;t}$ are associated with line ij to indicate the parent-child relationship between nodes i and j . In particular, if node j is the parent node of i , $b_{s;ij;t} = 1$, otherwise, $b_{s;ij;t} = 0$. The set of all power lines is denoted by E , and R denotes the set of root nodes.

Constraint (10) suggests that if line ij is connected, either node i or node j is the parent node. Constraints (11) and (12) indicate that the root node has no parent node, and each energized non-root node has exactly one parent node. Constraint (13) ensures that disconnected lines have no power flow.

In this problem, constraints (10) to (13) cannot eliminate the situation of pseudo root formation if some nodes can form local loops without violating the power balance constraint.

The formation of pseudo roots can lead to non-radial network topology. To address this issue, a small value (such as 0.00001 p.u) is added to the original load demand $P_{s;j;t}^l$ to create fictitious demands $P_{s;j;t}^{fl}$ that introduce errors in the original results. The nodal power balance constraint becomes:

$$P_{s;j;t}^{dg} + \sum_{i2'(j)} P_{s;ij;t} + P_{s;j;t}^m = P_{s;j;t}^{fl} + P_{s;j;t}^{gpp} + \sum_{i2(j)} P_{s;ji;t} \quad (14)$$

By adding a small positive value to the original load, it is guaranteed that all load nodes have positive demand. Thus, all load nodes must be connected to the root nodes through at least one power distribution path to supply their fictitious demands, thus, eliminating the possibility of pseudo-root formation. Together, constraints (10) to (14) can ensure the network radiality during the reconfiguration process.

The operation of gas-fired DGs is constrained by DG technical constraints (15) to (17):

$$P_{min}^{dg} \leq P_{s;j;t}^{dg} \leq P_{max}^{dg} \quad (15)$$

$$Q_{min}^{dg} \leq Q_{s;j;t}^{dg} \leq Q_{max}^{dg} \quad (16)$$

$$RD \leq P_{s;j;t+1}^{dg} - P_{s;j;t}^{dg} \leq RU \quad (17)$$

Constraints (15) and (16) give the gas-fired DG power limits. The ramping capability of DGs is constrained by (17), in which RD and RU denote the ramp-down and ramp-up limits of DGs.

2) Natural Gas System Constraints

In this work, the steady-state operation of a radial GN is modeled, and the gas well is the only gas source, as shown in Fig. 1. The nodal gas balance constraints for gas nodes $m \in M$ in the GN are as follows:

$$G_{s;m;t}^w = \sum_{n2\#(m)} F_{s;mn;t}^{act} + F_{s;mn;t}^{ina}; \delta_m \in W \quad (18)$$

$$G_{s;m;t}^l + G_{s;m;t}^{dg} = \sum_{n2(m)} F_{s;nm;t}^{act} + F_{s;nm;t}^{ina} \\ \times \sum_{n2\#(m)} F_{s;mn;t}^{act} + F_{s;mn;t}^{ina}; \delta_m \in B \quad (19)$$

The gas load, gas-fired DG fuel consumption, and gas well supply are denoted by $G_{s;m;t}^l$, $G_{s;m;t}^{dg}$ and $G_{s;m;t}^w$, respectively. The gas flows in active and inactive pipes are denoted by $F_{s;mn;t}^{act}$ and $F_{s;mn;t}^{ina}$, respectively. The sets of source nodes and non-source nodes are given by W and B , respectively. The parent and child node sets of node m are denoted as (m) and $\#(m)$, respectively. Constraints (18) and (19) are the nodal gas balance constraints for the source node and the non-source nodes, respectively.

The gas load loss is calculated using (20):

$$G_{s;m;t}^{loss} = G_{m;t}^0 - G_{s;m;t}^l \quad (20)$$

where $G_{m;t}^p$ represents the uninterrupted gas load for gas node m at time t .

In the GN, active gas pipes can drive gas flow and elevate the nodal pressure at the downstream node by operating the gas pumps. It is assumed that gas pumps are installed at necessary locations, and disruption in gas pump electricity supply will lead to gas load outages at downstream GN nodes.

$$0 \leq F_{s;mn;t}^{act} \leq U_{s;j;t} F_{max;mn}^{act} \quad (21)$$

$$U_{s;j;t} \delta_{s;m;t} \leq \delta_{s;n;t} \leq U_{s;j;t} \delta_{s;m;t} \quad (22)$$

The maximum gas flow in an active pipe mn is denoted by $F_{max;mn}^{act}$, and the binary variable $U_{s;j;t}$ is the activation status of the PDN node j that supplies electricity to the gas pump in pipe mn . The nodal pressures at the upstream and downstream nodes of the gas pipe mn are denoted as $\delta_{s;m;t}$ and $\delta_{s;n;t}$, respectively. $\delta_{s;n;t}$ is the maximum nodal pressure elevation capability of the gas pump.

Constraint (21) indicates that in active pipes, the gas flow can range between 0 and its maximum value as long as the gas pump has access to electricity. Constraint (22) is the nodal pressure elevation capability constraint of active pipes.

For inactive gas pipes, the gas flow depends on the nodal pressure difference between the end nodes. Since a radial GN is considered in this work, the gas flow is unidirectional. The gas flow in an inactive pipe mn can be modeled as:

$$(F_{s;mn;t}^{ina})^2 = \delta_{s;m;t}^2 - \delta_{s;n;t}^2 \quad (23)$$

$$0 \leq F_{s;mn;t}^{ina} \leq F_{max;mn}^{ina} \quad (24)$$

where β is the parameter for describing the relationship between gas flow and nodal pressure difference, and $F_{max;mn}^{ina}$ denotes the maximum gas flow in the inactive pipe mn .

3) Coupling Constraints

The interdependence between the PDN and the GN stems from the electricity consumption of gas pumps to drive gas flow in the GN, and the fuel consumption of gas-fired DGs to generate electricity in the PDN:

$$G_{s;m;t}^{dg} = c_{1;j} P_{s;j;t}^{dg} + c_{2;j} U_{s;j;t} \quad (25)$$

$$P_{s;j;t}^{gp} = \beta_{mn} F_{s;mn;t}^{act} \quad (26)$$

$$Q_{s;j;t}^{gp} = \% P_{s;j;t}^{gp} \quad (27)$$

where $c_{1;j}$ and $c_{2;j}$ are fuel consumption coefficients of the gas-fired DGs. Binary variables $U_{s;j;t}$ are the activation status of the PDN node j with gas-fired DGs. The gas pump electricity consumption coefficient is given by β_{mn} . Coefficient $\%$ is related to the power factor of gas pumps.

The coupling constraint (25) relates the gas-fired DG electricity generation $P_{s;j;t}^{dg}$ with the DG gas consumption $G_{s;m;t}^{dg}$. Constraints (26) and (27) relate the active pipe gas flow $F_{s;mn;t}^{act}$ with the gas pump electricity consumption.

4) Repair Crew Dispatching

A repair crew can travel through the TN to fix the damaged components after extreme events. In the restoration problem, the repair crew dispatching problem can be modeled as a vehicle routing problem that optimally routes the repair crew to visit and fix the faults $d \in D$. The repair crew routing problem can be modeled:

$$\sum_{h \in D} V_{h;d}^s = 1 \quad (28)$$

$$\sum_{h \in D} V_{h;d}^s = 1 \quad (29)$$

$$V_{d;d}^s = 0 \quad (30)$$

$$V_{h;d}^s + V_{d;h}^s \leq 1 \quad (31)$$

where the binary variable $V_{h;d}^s$ denotes the routing decision from fault h to fault d in scenario s , and $V_{h;d}^s = 1$ means that the repair crew chooses to move from fault h to fault d .

Constraints (28) and (29) restrict the number of times the repair crew flows into and out from each fault location, respectively. Together, constraints (28) and (29) ensure that each fault will be visited exactly once. Constraint (30) prohibits self-travels, and constraint (31) avoids sub-tours.

After the repair crew fixes the faults, the damaged components become available again. Hence, the fixing time $FT_{s;d}$ of fault d in scenario s should be modeled into the restoration problem to indicate the availability of damaged components.

$$AT_{s;d} \leq AT_{s;h} + V_{h;d}^s tt_{h;d} + V_{h;d}^s rt_h \quad (1 - V_{h;d}^s)M \quad (32)$$

$$FT_{s;d} = AT_{s;d} + rt_d \quad (33)$$

$$AT_{s;1} = 0 \quad (34)$$

$$\sum_{d \in D} U_{s;d;t} \leq T - FT_{s;d} \quad (35)$$

$$U_{s;d;t} \leq U_{s;d;t+1} \quad (36)$$

The arrival time at fault d is given by $AT_{s;d}$. The repair time of fault d is given by rt_d , and the travel time from fault h to fault d is denoted by $tt_{h;d}$. Notably, $AT_{s;d}$ and $FT_{s;d}$ are decision variables of the repair crew routing problem, $tt_{h;d}$ and rt_d are input parameters. The availability status of fault d is given by binary variables $U_{s;d;t}$.

Constraint (32) relates the arrival time $AT_{s;d}$ of fault d to the arrival time $AT_{s;h}$ of fault h that is visited right before d . Constraint (33) calculates the fixing time of fault d based on its arrival time $AT_{s;d}$ and required repair time rt_d . Constraint (34) indicates that the travel of the repair crew starts from the depot, which provides a boundary condition for calculating the fixing time of each fault. Constraints (35) and (36) restrict the availability of fault d until it is repaired.

5) Two-Stage MES Assigning and Dispatching

The MESs can be dispatched at both the pre-event and post-event stages through the TN, and pre-event dispatched

MESs can inject real and reactive power immediately after the restoration begins.

$$\sum_{j \in J} X_j + \sum_{j \in J} Y_{s;j} = N^m \quad (37)$$

$$X_j + Y_{s;j} = 1 \quad (38)$$

$$u_{s;j;t}^m P_{min}^m \leq P_{s;j;t}^m \leq u_{s;j;t}^m P_{max}^m \quad (39)$$

$$u_{s;j;t}^m Q_{min}^m \leq Q_{s;j;t}^m \leq u_{s;j;t}^m Q_{max}^m \quad (40)$$

$$E_{s;j;t+1}^m = E_{s;j;t}^m - \frac{P_{s;j;t}^m}{\eta} \Delta t \quad (41)$$

$$0 \leq E_{s;j;t}^m \leq E_{max}^m \quad (42)$$

$$u_{s;j;t}^m = X_j \quad (43)$$

$$u_{s;j;t}^m = (T - tt_{1;j}) Y_{s;j} + X_j \quad (44)$$

$$u_{s;j;t}^m = u_{s;j;t+1}^m \quad (45)$$

The total number of MES is N^m . The binary variable $u_{s;j;t}^m$ indicates if an MES is available for node j at time t in scenario s . P_{min}^m , P_{max}^m , Q_{min}^m , and Q_{max}^m denote MES power limits. The MES energy content is denoted by $E_{s;j;t}^m$ and the full MES energy capacity is given by E_{max}^m . The MES discharging efficiency is denoted by η . The transportation time of MES from the depot to node j is given by $tt_{1;j}$.

Constraint (37) restricts the total number of MES dispatched at both the preparation and restoration stages. Constraint (38) ensures that MES will not be repeatedly dispatched to the same location. Constraints (39) to (42) are MES power and energy constraints. The MES availability status is constrained by constraints (43) to (45). Constraint (43) indicates that if an MES is dispatched to node j at the pre-event stage, it is always available at node j . Constraints (44) and (45) ensure that a post-event dispatched MES can only begin to inject power after its arrival.

Notably, the dispatching decisions X_j and $Y_{s;j}$ only indicates if an MES is dispatched to node j at the pre-event or post-event stage. The availability of MES for node j at time t is represented by $u_{s;j;t}^m$, which depends on the MES dispatching decisions (X_j and $Y_{s;j}$) and the travel time $tt_{1;j}$ from the depot to node j , as indicated in constraints (43) and (44). Specifically, if an MES is dispatched to node j at the pre-event stage ($X_j = 1$), it can begin to work immediately as the restoration begins ($u_{s;j;t}^m$ can be set to 1 in the first time slot of the post-event stage). If an MES is dispatched to node j at the post-event stage ($Y_{s;j} = 1$), it can only begin to work after it travels from the depot to node j ($u_{s;j;t}^m$ cannot be set to one until the time slot that is larger than the travel time $t - tt_{1;j}$). As shown in eqs (37) – (45), the proposed unified preparation and restoration model not only explicitly incorporates the MES dispatching and operation constraints at both pre- and post-event stages but also effectively addresses the coupling

between two stages, which enables unified optimization of both stages to maximize the load restoration efficiency.

By solving the pre-event preparation problem, the MES assigning and pre-event dispatching problems are solved, and the pre-event MES dispatching solution X_j is implemented.

B. Post-Event Optimal Restoration

In the post-event restoration stage, the damage information becomes known parameters, and the pre-event MES dispatching has been completed. The post-event restoration problem optimally coordinates all the resilience resources to minimize load loss in both the PDN and the GN.

$$\min_{Y_j, u_j; t; Z_t^e; Z_t^g; R} \sum_{t \in T} \sum_{j \in J} w_j^e P_{j;t}^{loss} + \sum_{t \in T} \sum_{m \in M} w^g G_{m;t}^{loss} + W^{ft} \sum_{d \in D} FT_d \quad (46)$$

s.t.

$$\text{Power System Constraints} \quad (47)$$

$$\text{Natural Gas System Constraints} \quad (48)$$

$$\text{Power - Gas Coupling Constraints} \quad (49)$$

$$\text{Repair Crew Constraints} \quad (50)$$

$$\text{MES Constraints} \quad (51)$$

IV. SOLUTION METHODOLOGY

To ensure the quality of the preparation decision under the damage uncertainty, multiple fault scenarios should be simulated at the pre-event stage. However, the two-stage stochastic optimization model generates one set of decision variables and constraints for each fault scenario, which significantly increases the problem dimension. To efficiently solve the formulated optimal preparation problem considering a reasonable number of fault scenarios, a distributed solution method is developed in this section based on a proposed selective PH algorithm.

A. Distributed Solution Method

For a finite number of fault scenarios, the two-stage stochastic problem is a single-stage mixed-integer linear programming problem, in which a set of decision variables and constraints are duplicated for each generated scenario. Based on the PH algorithm, the original problem can be decomposed into a primary problem and multiple secondary problems. The primary problem coordinates the results obtained by solving all secondary problems. Besides, each secondary problem is responsible for calculating the optimal preparation and restoration solutions for one of the generated scenarios based on the primary problem coordination result. After the decomposition, the secondary problems can be written as:

$$\min_{X_j^s; Y_j; u_j; t; Z_t^e; Z_t^g; R} \sum_{t \in T} \sum_{j \in J} w_j^e P_{j;t}^{loss} + \sum_{t \in T} \sum_{m \in M} w^g G_{m;t}^{loss} + W^{ft} \sum_{d \in D} FT_d + \sum_{s; 1} X_j^s + \frac{1}{2} \sum_{X_j^s} X_j^p + \sum_{X_j^p} X_j^p \quad (52)$$

subject to constraints (2) to (45).

In formulation (52), $X_{j_i}^S$ is the optimal pre-event MES dispatching decision of secondary problems in iteration i . The coordinated pre-event MES dispatching result in the previous iteration is given by $X_{j_i}^{p_{i-1}}$. The penalty coefficient for coordinating the secondary problems is given by $\lambda_{j_i}^S$. The dual multiplier of the secondary problem for scenario S in iteration i is denoted by μ_{S_i} . In this formulation, by adding the penalty terms, it is ensured that the secondary problems would account for the deviation from the coordinated pre-event MES dispatching result $X_{j_i}^{p_{i-1}}$ while making the optimal pre-event MES dispatching decisions $X_{j_i}^S$.

The primary problem for coordinating the secondary problem results in iteration i can be written as:

$$X_{j_i}^p = \sum_{S \in \mathcal{S}} \mu_{S_i} X_{j_i}^S \quad (53)$$

where $X_{j_i}^S$ are the optimal pre-event MES dispatching decisions obtained from the secondary problems in iteration i .

After obtaining the pre-event MES dispatching results from both the primary and secondary problems, the dual multiplier for each secondary problem in iteration i can be updated as:

$$\mu_{S_i} = \mu_{S_{i-1}} + \lambda_{j_i}^S (X_{j_i}^p - X_{j_i}^S) \quad (54)$$

The problem is considered converged when the differences between the pre-event MES dispatching solutions of primary and secondary problems are smaller than a given threshold ϵ .

$$\sum_{S \in \mathcal{S}} \mu_{S_i} (X_{j_i}^p - X_{j_i}^S)^2 \leq \epsilon \quad (55)$$

Notably, in the first iteration, the secondary problems would optimize the MES dispatching without considering the deviation penalty. But for all other iterations, the penalty terms should be included:

$$\mu_{S_i} = 0 \quad \mu_{S_{i-1}} = 1 \quad (56)$$

B. Proposed Selective Progressive Hedging Algorithm

The conventional PH algorithm requires solving all scenarios in each iteration to update the first-stage decision. In addition, some biased scenarios with optimal first-stage decisions significantly different from the majority require more iterations to converge. Hence, it is computationally intensive if all scenarios are treated equally and solved for multiple iterations due to the slow convergence of certain biased scenarios. Although this additional computational burden does not lead to additional computational time if the computer has enough workers and memory to process all the scenarios in parallel, most computers have limited computational resources. Hence, scenarios cannot be processed simultaneously, but need to be divided into batches and solved sequentially. Consequently, additional computational time will be needed due to the existence of biased scenarios. Recognizing that these biased scenarios are the primary bottlenecks hindering the convergence of the distributed solution method, this work proposes a selective PH algorithm to accelerate the convergence by selectively focusing on solving such biased scenarios to reduce the computational

burden.

The conventional PH algorithm updates the first-stage decision by solving all scenarios in each iteration i , which does not support selectively focusing on biased scenarios. To address this issue, the conventional PH algorithm is modified such that in each iteration, only a subset of scenarios \mathcal{S}_i need to be solved to update the first-stage decisions using eq (53). In addition, to fully utilize the computational resource, the size of subsets \mathcal{S}_i in each iteration is set to the number of workers n_w of the computer (assuming adequate memory). By reducing the number of scenarios solved in each iteration, the proposed selective PH algorithm provides the flexibility to enable targeted focus on biased scenarios that require additional iterations to converge.

To achieve targeted resolution of biased scenarios, a selective sampling mechanism is developed to prioritize scenarios with higher bias in each iteration. This is accomplished by focusing on scenarios that exhibit greater deviations from the coordinated first-stage decisions when selecting scenarios to be solved in each iteration i . These scenarios are typically more biased and take more iterations to converge. To identify and sample these biased scenarios for resolution, the deviations D_{S_i} between the first-stage decisions $X_{j_i}^S$ of each scenario S and the coordinated first-stage decision $X_{j_i}^p$ are calculated using (57):

$$D_{S_i} = \sum_{j \in \mathcal{J}} \frac{\mu_{S_i} (X_{j_i}^S - X_{j_i}^p)^2}{\sum_{j \in \mathcal{J}} \mu_{S_i} (X_{j_i}^S - X_{j_i}^p)^2} \quad (57)$$

Based on the deviations of different scenarios, the probability Pr_{S_i} of scenario S to be sampled in the scenario subset in each iteration i is calculated using eq (58):

$$Pr_{S_i} = \frac{\mu_{S_i} D_{S_i}}{\sum_{S \in \mathcal{S}} \mu_{S_i} D_{S_i}} \quad (58)$$

Following eqs (57) and (58), scenarios with greater bias are assigned higher probabilities for selection in each iteration. Subsequently, a total of n_w scenarios are sampled from the scenario set \mathcal{S} using the sampling probabilities Pr_{S_i} derived in eq (58). The selected scenarios are then resolved to update the first-stage decisions $X_{j_i}^p$ in iteration i . Additionally, the dual multipliers corresponding to the selected scenarios are updated using equation (54). Notably, to ensure that all scenarios are initially solved without penalty terms, the scenario selection process commences after the first iteration, thereby guaranteeing an unbiased initial solution.

To this end, the developed distributed solution algorithm can be summarized as follows:

V. CASE STUDY

In this section, numerical results are presented to evaluate the benefit of using MES in the restoration process and validate the performance of the proposed methods.

A. Experiment Setup

The investigated IEGDS consists of a 69-node PDN and a 7-node GN, as shown in Fig. 2. Gas-fired DGs are installed at PDN nodes 32 and 38, and one active pipe is constructed in the GN. There are five normally open tie-lines, whose positions

Algorithm 1 Selective PH algorithm

- 1: Set $\alpha = 1$, $\beta = 10^{-3}$, $\gamma = 1$, $\delta = 0$, $\epsilon = S$.
- 2: For each selected fault scenario $s \in \mathcal{S}$, solve problem (52) to derive $X_{f_j}^s$.
- 3: Calculating pre-event MES dispatching coordination result $X_{f_j}^p$ using (53)
- 4: Verify convergence by checking if (55) is satisfied
- 5: **if** (55) is not satisfied **then**
- 6: Update the dual multipliers for $s \in \mathcal{S}$ using (54)
- 7: Calculate the deviations D_s for $s \in \mathcal{S}$ using (57)
- 8: Compute sampling probabilities for $s \in \mathcal{S}$ using (58)
- 9: Sample n_w scenarios from \mathcal{S} based on Pr_s
- 10: Go back to step (2)
- 11: **else**
- 12: Terminate the iteration
- 13: Output the pre-event MES dispatching decision $X_{f_j}^p$
- 14: **end if**

are indicated in Fig. 2. The depots for the repair crew and MESs are located close to the substation. The travel time from the depot to different locations ranges between 0.2 and 2.5 hours. The number of MES is set to 5. The MES power and energy ratings are 500kW and 1,000kWh, respectively. The MES discharging efficiency is set to 0.95. The power limit of the gas-fired DGs is 1,000kW. The optimization horizon is 12 hours, and the optimization resolution is 0.5 hour. It is assumed that only power lines will be damaged, and the repair time for each damaged line is set to 1 hour. The uninterrupted electric and gas loads are shown in Fig. 3. The total electricity demand during the restoration process is 96.426 MWh, and the total gas demand is 15,164 m^3 .

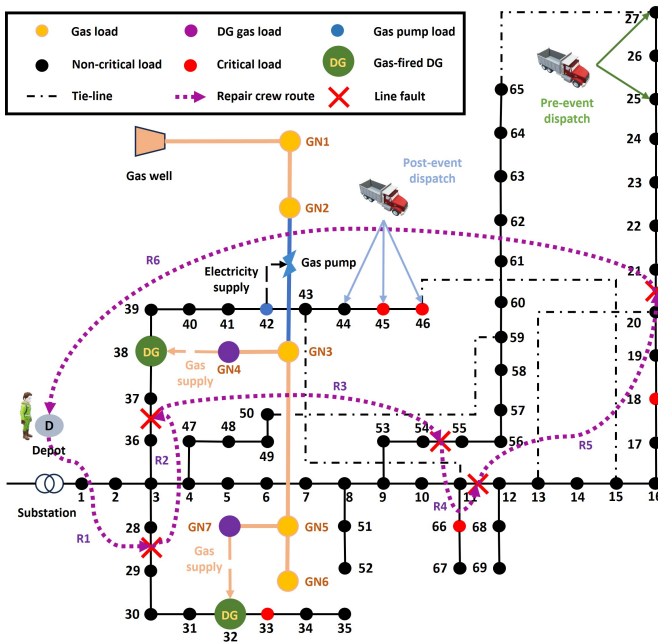


Fig. 2: System topology, fault scenario, MES dispatching, and repair crew routing

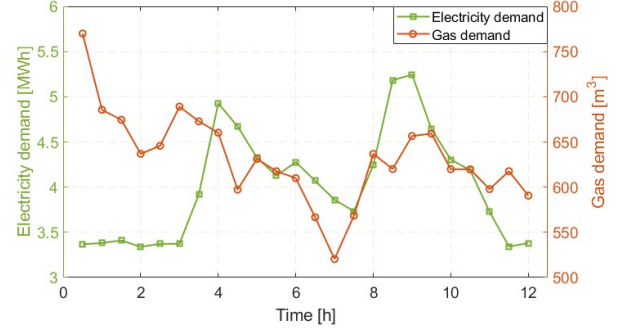


Fig. 3: Electricity and gas load curves

B. Numerical Results

An illustrative fault scenario, the pre-event MES dispatching, and the post-event MES dispatching results are displayed in Fig. 2. In the pre-event stage, two MESs are dispatched to nodes 25 and 27, respectively. The pre-event MES dispatching result can be explained from three aspects. Firstly, because nodes 25 and 27 are located very far from the depot, it costs a lot of time for MES to transport from the depot to nodes 25 and 27. Hence, dispatching MES to these nodes is more efficient in terms of the time-saving advantage of pre-event MES dispatching. Secondly, the feeder that contains nodes 25 and 27 is the longest feeder in the PDN, making the nodes on this feeder more likely to experience low-voltage problems during the restoration process. Therefore, dispatching MES to the far end of this feeder can improve the restoration efficiency by providing voltage support to avoid potential voltage violations. In addition, the feeder containing nodes 25 and 27 is interconnected with other feeders through tie-lines 15-46 and 27-65. Because these two tie-lines connect this feeder to the far ends of two other feeders, more severe voltage drop and line congestion can occur if these tie-lines are closed during the reconfiguration process. To facilitate potential reconfiguration operations involving these tie-lines, MESs are strategically dispatched to nodes close to these tie-lines. As a combined result of these considerations, the proposed strategy dispatches MES to nodes 25 and 27 at the preparation stage to enhance system preparedness.

After the fault scenario shown in Fig. 2 is revealed, the proposed strategy coordinates all the resilience resources to restore load outages. The fastest operation is closing remotely controllable tie-lines to swiftly switch the interrupted load to alternative feeders. In this case, tie-lines 11-43, 27-65, and 50-59 are closed immediately after the restoration begins. By closing these tie-lines, the energy supply at nodes 21 to 27, nodes 37 to 46, and nodes 55 to 65 are restored. Because the electricity of the gas pump is supplied by node 42, the gas supply in the GN is also restored by operating tie-lines.

Notably, there is a tie-line connecting node 46 to node 15. However, this tie-line is not closed even if the energy supply on node 46 has been restored. Tie-line 15-46 is kept open because the voltage on node 46 is very close to the lower limit, connecting more loads through tie-line 15-46 will cause voltage violations. To address this problem, the rest MESs are dispatched to nodes 44, 45, and 46 to provide voltage support by injecting power. After post-event dispatched MESs arrive

at $t = 3$, tie-line 15-46 is closed at $t = 4$ and the energy supply of nodes 12 to 20, 68, and 69 is restored.

Similarly, without the power injection from pre-event dispatched MES at nodes 25 and 27, closing tie-line 27-65 would also lead to voltage violations because the energy supply for nodes 21 to 27 relies on an extended power distribution path after reconfiguration. However, the strategic pre-event deployment of MESs to nodes 25 and 27 enables immediate power injection upon the commencement of the restoration process. Consequently, tie-line 27-65 can be closed earlier than tie-line 15-46. The latter must remain open until power injection from post-event dispatched MES is available. This contrast demonstrates the significance of the pre-event MES dispatching in improving the restoration efficiency.

The power injections of MESs are summarized in Fig. 4(a). Specifically, pre-event dispatched MESs can inject power immediately after the restoration begins, ensuring a prompt contribution to the restoration process. For post-event dispatched MESs, power injections commence upon their arrival at designated locations with a higher utilization rate compared to pre-event dispatched MESs. The pre-event and post-event dispatched MES power injection features reflect the coordination within the proposed MES deployment strategy.

Following the fuel supply restoration, gas-fired DGs can inject power to mitigate voltage drop and line congestion problems. As illustrated in Fig. 4(b), the DG located at node 38 initiates power injection once tie-line 15-46 is closed. The DG at node 32 is not injecting power before its feeder is restored because the islanded operation is unavailable in this work. After this feeder is restored, the DG at node 38 is still not injecting power because nodal voltages on this feeder can be maintained without requiring additional support from the DG.

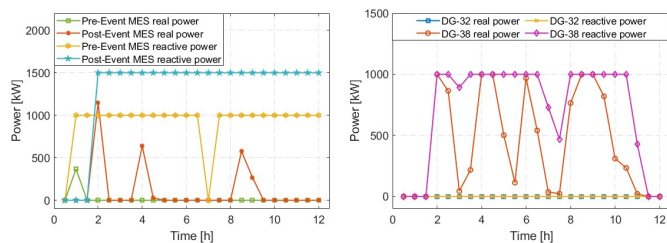


Fig. 4: (a) MES power injection (b) DG power injection

By operating tie-lines, MESs, and gas-fired DGs, the majority of load outages can be successfully restored. Meanwhile, the repair crew is dispatched to fix fault lines and restore the remaining load outages. The repair crew route is visualized in Fig. 2 using dashed arrows. In this case, the load on nodes 29 to 35 is interrupted because of the fault on line 28-29, and the energy supply on these nodes can only be restored by fixing line 28-29. Hence, the repair crew is routed to repair fault line 28-29 first. By fixing this fault line, nodes 29 to 35 are restored, thereby resolving all load outages. However, the repair crew proceeds to repair the remaining fault lines, following the shortest path to minimize the overall fixing time.

The load restoration process is summarized in Table II. In Table II, nodes 37 to 46, and nodes 55 to 65 can be

restored immediately by closing tie-lines. Besides, following the restoration of node 42, the gas supply of gas nodes 3 to 7 in the GN is also restored because the electricity supply to the gas pump is restored. Further, nodes 21 to 27 can be immediately restored by closing tie-lines thanks to the voltage support provided by pre-event dispatched MESs. In contrast, the energy supply of nodes 12 to 20, 68, and 69 remains interrupted until MESs arrive at nodes 44, 45, and 46 at the post-event stage. This delay reduces the restoration efficiency by increasing 1.104 MWh of electric load loss.

TABLE II: Restoration Process Summary

Restored nodes	Restoration time	Restoration operation
37 to 46, gas nodes 3 to 7	2	Closing tie-line 11-43
55 to 65	2	Closing tie-line 50-59
21 to 27	2	Closing tie-line 27-65, pre-event dispatched MES power injection
12 to 20, 68, 69	4	Closing tie-line 15-46, post-event dispatched MES power injection, gas-fired DG power injection
29 to 35	4	Repair crew fixing fault line 28-29

The system reconfiguration after the restoration is shown in Fig. 5. To minimize the load loss, 4 tie-lines are closed, indicated as green lines in Fig. 5. Meanwhile, 4 damaged power lines are left open in the reconfigured network, indicated as dotted blue lines. Notably, for the fault line 28-29, there is no tie-line capable of switching the load affected by this fault to alternative feeders. Hence, line 28-29 is reconnected after the fault is repaired.

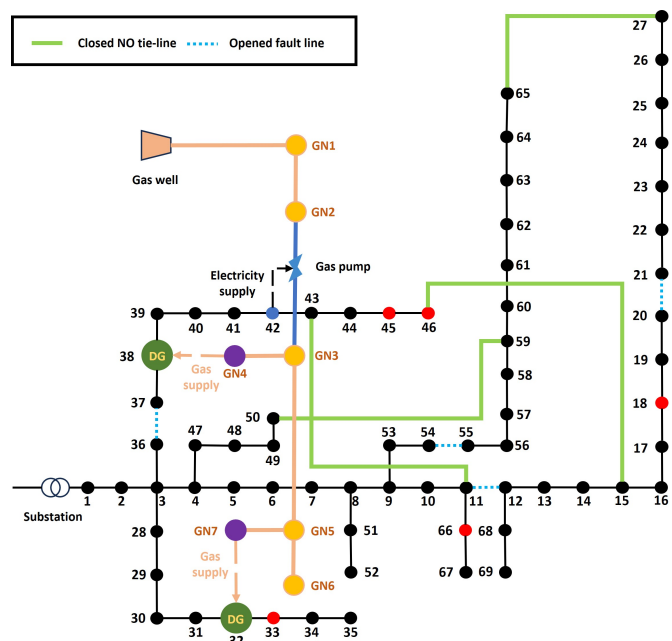


Fig. 5: System reconfiguration after the restoration process

To evaluate the benefits of using MES and assess the performance of the proposed methods, five different strategies

are investigated in this work, and their restoration results are consolidated in Table. III.

Strategy 1: No MES is available in both stages.

Strategy 2: MESs are exclusively dispatched in the pre-event stage, while other conditions remain unchanged.

Strategy 3: MESs are solely dispatched in the post-event stage, and the restoration strategy remains unchanged.

Strategy 4: MES are pre-positioned to candidate buses and rerouted to optimal buses at the post-event stage [35].

Strategy 5: The proposed strategy.

In strategy 1, the absence of MES renders nodes 12 to 20, 68, and 69 unrecoverable using tie-lines. Instead, fault line 11-12 is repaired to restore these nodes. Besides, because of system reconfiguration, repaired line 11-12 can only be closed at the last moment of the restoration process, which leads to a huge loss of electric load. Furthermore, due to voltage violations, tie-line 27-65 can only be closed at $t = 4$, further increasing the electric load loss.

In strategy 2, using the same fault scenarios and solution method, MESs are dispatched to nodes 22, 24, 25, 26, and 27 at the pre-event stage. Despite the power support from pre-event dispatched MES is available, tie-line 27-65 is not immediately closed to restore nodes 21 to 27. Instead, fault line 20-21 is repaired at $t = 9$, then closed simultaneously with tie-line 15-46 at $t = 10$. Consequently, nodes 12-20, 68, and 69 are restored together with nodes 21 to 27 at $t = 10$. This severe delay results in a substantial electric load loss.

In strategy 3, MESs are dispatched to nodes 41, 43, 44, 45, and 46 at the post-event stage. In this strategy, the reconfiguration result is the same as the proposed strategy. However, because no MES is available to maintain the voltage of nodes 21 to 27 at the beginning of the restoration, tie-line 27-65 can only be closed at $t = 4$ after the post-event dispatched MESs arrive. As a result, the load loss is increased by 0.616 MWh compared to the proposed strategy.

In strategy 4, all terminal buses and buses with more than two child buses (including tie-line buses) are selected as the candidate buses. In the pre-event stage, MESs are pre-positioned at buses 11, 27, 65, 67, and 69. In the post-event stage, the MESs that are pre-positioned at buses 11 and 65 are rerouted to buses 43 and 46, and other pre-positioned MESs remain unchanged. Because of the power and energy support provided by pre-positioned MESs at buses 27, 67, and 69, the tie-line 27-65 is closed immediately after the restoration begins to pick up loads. In addition, tie-lines 11-43 and 50-59 are also immediately closed without violating network constraints. However, due to the rerouting process of MESs from buses 11 and 65 to buses 43 and 46, tie-line 15-46 is closed at $t = 5$ after the rerouted MESs arrive, which leads to an additional electric load loss of 0.328 MWh.

The electric load loss of all strategies is summarized in Fig. 6. Besides, the gas load loss is the same for all strategies because the energy supply of the gas pump can be restored by closing the tie-line 11-43 immediately without causing violations.

In the developed distributed solution method, the penalty coefficient is set to 0.5. By simulating 50 fault scenarios in the preparation stage, the problem converges after 6 iterations.

TABLE III: Restoration Results Comparison

Strategy	Electric load loss (MWh)	Gas load loss (m^3)	Pre-event MES dispatching	Post-event MES dispatching	Closed fault-lines and tie-lines
1	18.449 (100%)	660	/	/	11-12,28-29, 11-43,27-65, 50-59
2	10.844 (58.78%)	660	22,24,25, 26,27	/	20-21,28-29, 11-43,15-46, 50-59
3	4.795 (25.99%)	660	/	41,43,44, 45,46	28-29,11-43, 15-46,27-65, 50-59
4	4.5066 (24.42%)	660	11,27,65 67, 69	27,43,46 67, 69	28-29,11-43, 15-46,27-65, 50-59
5	4.179 (22.65%)	660	25,27	44,45,46	28-29,11-43, 15-46,27-65, 50-59

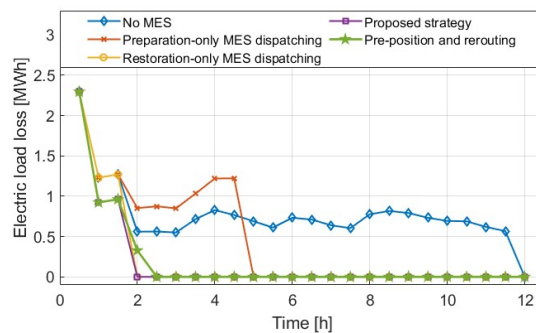


Fig. 6: Electric load loss comparison

The pre-event MES dispatching probability convergence process obtained from the developed distributed solution method is displayed in Fig. 7.

In the first iteration, there is no penalty term accounting for pre-event MES dispatching deviations in secondary problems, making all secondary problems prefer to pre-dispatch MES to maximize the restoration efficiency. This leads to diversified pre-event MES dispatching solutions due to the diversity of fault scenarios. However, certain PDN nodes are preferred for MES dispatching in the first iteration. From Fig. 7, it can be observed that nodes 11 to 27, nodes 44 to 46, and nodes 56 to 65 are favored MES dispatching locations. Specifically, there is an increasing trend in MES dispatching probability as the distance between PDN nodes and the substation increases, indicating a correlation between the length of the power distribution path and MES dispatching preference.

As the problem iterates, the pre-event MES dispatching probabilities of nodes 25 and 27 gradually increase to 1, as highlighted in Fig. 7. This result suggests that pre-dispatching MESs to these two nodes offers the optimal trade-off between MES transportation time and dispatching accuracy. This result also gives the MES assigning solution, as only nodes 25 and 27 have MES dispatched in the pre-event stage. Conversely, the pre-event MES dispatching probabilities of other nodes decrease to 0 as the problem iterates, indicating that the time saved by pre-dispatching MESs cannot balance the dispatching accuracy loss for other nodes.

To evaluate the performance of the proposed selective PH algorithm, different problem sizes are tested for both the

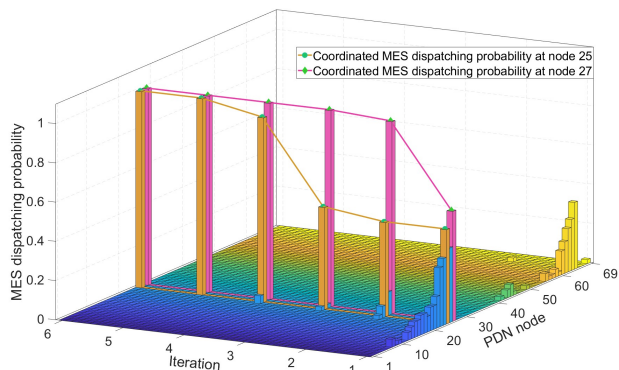


Fig. 7: Pre-event MES dispatching probability convergence process proposed selective PH and standard PH algorithms. The tested problem sizes include 16, 32, 48, and 64 fault scenarios. Fig.8 shows the convergence process and the solution time for each secondary problem of both algorithms under different problem sizes. Compared to the standard PH algorithm, the proposed selective PH algorithm updates the coordinated first-stage decision more efficiently and converges by solving fewer secondary problems across all simulated problem sizes. Specifically, the standard PH algorithm requires solving 96, 128, 192, and 320 secondary problems to converge for the respective problem sizes, whereas the proposed selective PH algorithm requires solving 56, 96, 176, and 280 secondary problems to converge. Due to the reduced number of solved secondary problems for convergence, the total solution time is reduced by 30.53% (from 5191.8s to 3606.9s), 22.23% (from 5563.8s to 4327.2s), 7.23% (from 10394.1s to 9643.4s), and 15.65% (from 16983.6s to 14325.4s) for problem sizes with 16, 32, 48, and 64 scenarios, respectively.

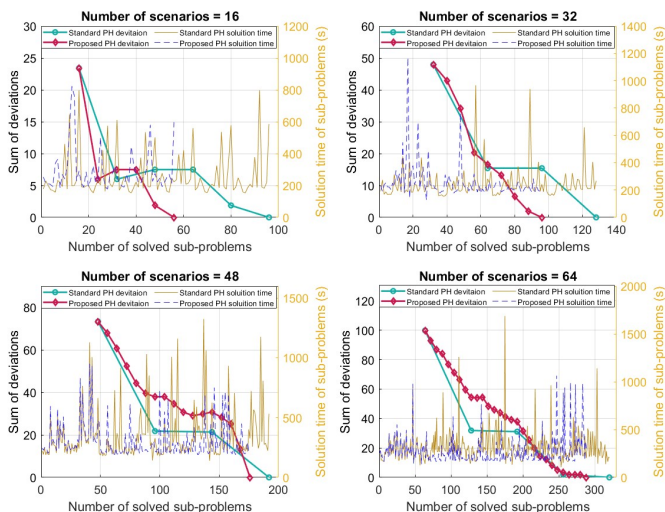


Fig. 8: Convergence of different algorithms under different problem sizes

C. Out-of-Sample Analysis

To further validate the superiority of the proposed methods, the out-of-sample analysis is performed by testing 1,000 fault scenarios for all the discussed strategies. The load loss results are displayed in Fig. 9. By comparing the results of strategies

1 and 5, the value of utilizing MES for enhancing IEGDS resilience can be demonstrated by observing an average of 53.10% and 2.85% of electric and gas load loss reductions, respectively. Besides, as compared to preparation-only and restoration-only MES dispatching strategies, the average electric load loss of the unified MES assigning and dispatching strategy is reduced by 2.65% and 7.13%, respectively. By comparing the results of strategies 4 and 5, it is observed that the pre-positioning and rerouting strategy has a similar performance in restoring the electric load compared to the proposed strategy. However, the proposed strategy outperforms the pre-positioning and rerouting strategy for gas load restoration, as shown in Fig. 9(b). Compared to the pre-positioning and rerouting strategy, the proposed strategy can reduce the average electric and gas load losses by 0.12% and 1.43%, respectively.

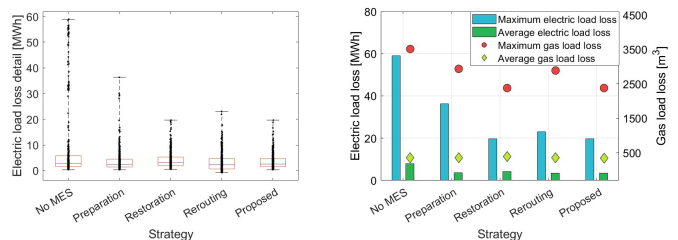


Fig. 9: (a) Electric load loss details (b) Load loss summary

D. Sensitivity Analysis

In this problem, the fault repair time and travel time are crucial to the restoration efficiency. Some faults can take a longer time to repair, which can delay the restoration. Besides, transportation conditions after extreme events may degrade, which can hinder the deployment of MES and the repair crew. To analyze the impacts of these factors on the restoration efficiency, sensitivity analysis is performed to evaluate the impacts of different time parameters on the restoration efficiency, as shown in Fig. 10. The load restoration results under different fault repair times are displayed in Fig. 10(a) using 100 fault scenarios. Because some faults can take a longer time to repair, the scheduling horizon is extended to 24 hours in the sensitivity analysis. In Fig. 10(a), the repair time ranges from 0.5 hours to 4 hours. It can be observed that the load loss increases with increased repair time. By increasing the fault repair time from 0.5 hour to 4 hours, the average electric load loss has been increased by 86.8% (from 3.895 MWh to 7.275 MWh), and the average gas load loss has been increased by 60.2% (from 352.417 m^3 to 564.710 m^3)

Further, to assess the impact of post-event travel time on restoration efficiency, different travel times (25% to 200% of the original post-event travel time) are tested. The pre-event MES dispatching results are summarized in Table. IV. When travel time is not significant, no MES is dispatched at the pre-event stage because MES can be dispatched quickly and accurately at the post-event stage without affecting the restoration efficiency. As the travel time increases, the impact of post-event MES dispatching travel time becomes significant and the proposed strategy prefers to dispatch more MES at the

pre-event stage for larger travel time (2 pre-event dispatched MES when travel time is 50% of the original value to 4 pre-event dispatched MES when travel time is 200% of the original value). In addition, the pre-event dispatched MESs are all located on nodes 22 to 27, which are nodes located at the farthest end of the feeder. The load loss results of 100 damage scenarios under different travel time settings are summarized in Fig. 10(b). When travel time is minimal, the load loss remains low even without pre-event deployment of MES. As the travel time increases, the average electric load loss surges by 468.3% (from 2.241 MWh to 12.735 MWh), and the average gas load loss is increased by 75.5% (from 436.148 m^3 to 765.620 m^3).

The sensitivity analysis reveals that travel time has a more profound impact on restoration efficiency compared to fault repair time. This is attributed to the fact that, in most instances, interrupted loads can be restored through local generations and tie-lines, whereas fault repair time primarily affects loads that rely on specific fault repairs for restoration. Moreover, travel time not only hinders fault repair efficiency by delaying repair crews but also influences the deployment of MESs, which plays a crucial role in providing power support for restoring interrupted loads in this work.

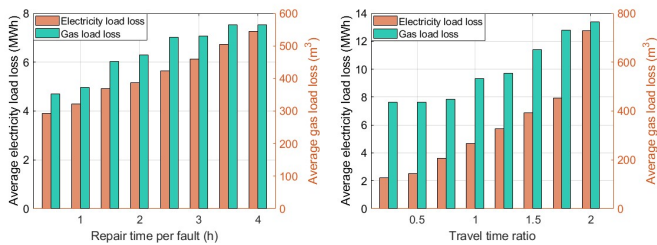


Fig. 10: Sensitivity analysis for (a) fault repair time (b) travel time

TABLE IV: Pre-Event MES Dispatching Summary

Ratio to the original travel time	Pre-event MES Dispatching	Number of pre-event dispatched MES
25%	/	0
50%	26, 27	2
75%	24, 25, 26	3
100%	25, 27	2
125%	24, 25, 27	3
150%	24, 25, 27	3
175%	22, 24, 25, 27	4
200%	22, 24, 26, 27	4

E. Scalability Analysis

To evaluate the scalability of the proposed restoration strategy, a larger system consisting of 141 PN nodes and 12 GN nodes is studied, as shown in Fig. 11. In the pre-event stage, MESs are dispatched to nodes 128, 130, and 141. These nodes are typically located far from the substation and close to the tie-line 32-130, which enables them to maximize the utilization of MES like in the 69-node system. Although there is a gas-fired DG (at node 140) located very close to the pre-event MES dispatching nodes, this DG is very likely to experience

fuel supply interruptions if either of the two gas pumps cannot work properly.

The fault scenarios and repair crew routing are also displayed in Fig. 11. After the faults occur, tie-line 32-130 is closed to restore nodes 22 to 32, 140, and 141 with the power support of pre-event dispatched MES. Meanwhile, the repair crew first repairs the fault line 91-101 to restore nodes 101 to 106. Then, the fault line 47-83 is repaired to restore the critical load on node 83. Further, fault lines 5-35 and 7-111 are sequentially repaired to restore nodes 35 and 111. Line 21-22 is the last repaired fault because the interrupted nodes due to this fault are already restored by connecting tie-line 32-130. In addition, the remaining MESs are dispatched to nodes 106 and 129 at the post-event stage to provide power support.

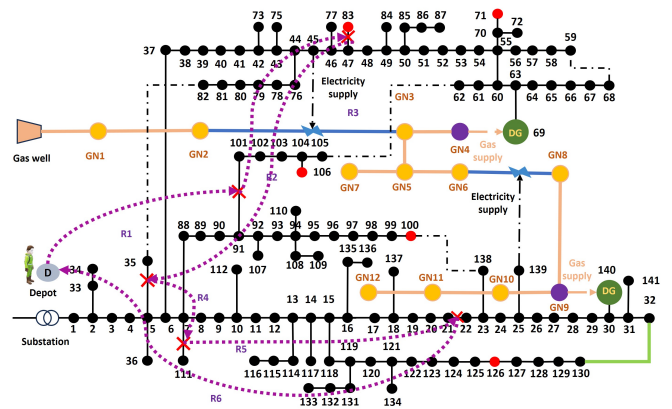


Fig. 11: The 141 node system

The case studies are simulated on Matlab using the Yalmip toolbox and GUROBI solver. The computer has 16 GB RAM, and the CPU is AMD R7 5800H with 8 workers solving the secondary problems in parallel. The solution time for both 69-node and 141-node cases are summarized in Table.V under 50 fault scenarios. For the 69-node and 141-node systems, the average solution time per fault scenario in the pre-event preparation stage is 339.98 s and 760.86 s, respectively. The total solution time of the 69-node system is 13478.12 s (3.74 hours) and the total solution time of the 141-node system is 29031.87 s (8.06 hours). Such computation times are acceptable because the preparation stage usually needs to start earlier before the extreme events. In addition, the post-event solution times of the 69-node and 141-node systems are 203.36 s and 394.54 s, respectively.

TABLE V: Computation Time Summary

System	Minimum time (s)	Maximum time (s)	Average time (s)	Total solution time
69-node	112.83	1022.53	339.98	13478.12 s (3.74 hours)
141-node	282.35	1545.57	760.86	29031.87 s (8.06 hours)

VI. CONCLUSION

This paper aims to improve the resilience of IEGDSs by efficiently utilizing MES for both pre-event preparation and post-event restoration. Employing MES, even with simple

preparation-only and restoration-only dispatching strategies, can significantly reduce electric load loss by 50.45% and 45.97%, respectively. Considering the trade-off between MES transportation time and dispatching accuracy, a unified MES assigning and dispatching strategy is proposed, which can further reduce the electric load loss by 2.65% and 7.13% compared to preparation-only and restoration-only strategies, respectively. Overall, as compared to the scenario without MES, the proposed method reduces an average of 53.10% and 2.85% of electric and gas load loss, respectively. Based on the methods proposed in this work, one possible future extension can be optimal planning of MES sizing and numbers. Besides, properly aggregated electric vehicles can provide similar functionalities as MES. Hence, efficiently guiding electric vehicles to enhance system resilience can also be a future research direction.

REFERENCES

- [1] C. Lv, R. Liang, W. Jin, Y. Chai, and T. Yang, "Multi-stage resilience scheduling of electricity-gas integrated energy system with multi-level decentralized reserve," *Applied Energy*, vol. 317, p. 119165, 2022.
- [2] R. P. Liu, S. Lei, C. Peng, W. Sun, and Y. Hou, "Data-based resilience enhancement strategies for electric-gas systems against sequential extreme weather events," *IEEE Transactions on Smart Grid*, vol. 11, no. 6, pp. 5383–5395, 2020.
- [3] M. Sang, Y. Ding, M. Bao, S. Li, C. Ye, and Y. Fang, "Resilience-based restoration strategy optimization for interdependent gas and power networks," *Applied Energy*, vol. 302, p. 117560, 2021.
- [4] B. Li, Y. Chen, W. Wei, Z. Wang, and S. Mei, "Online coordination of lng tube trailer dispatch and resilience restoration of integrated power-gas distribution systems," *IEEE Transactions on Smart Grid*, vol. 13, no. 3, pp. 1938–1951, 2022.
- [5] J. Yun, Z. Yan, Y. Zhou, P. Zhang, and W. Hu, "Multi-time collaborative restoration for integrated electrical-gas distribution system based on rolling optimization," *CSEE Journal of Power and Energy Systems*, 2020.
- [6] J. Li, Y. Xu, Y. Wang, M. Li, J. He, C.-C. Liu, and K. P. Schneider, "Resilience-motivated distribution system restoration considering electricity-water-gas interdependency," *IEEE Transactions on Smart Grid*, vol. 12, no. 6, pp. 4799–4812, 2021.
- [7] G. Li, K. Yan, R. Zhang, T. Jiang, X. Li, and H. Chen, "Resilience-oriented distributed load restoration method for integrated power distribution and natural gas systems," *IEEE Transactions on Sustainable Energy*, vol. 13, no. 1, pp. 341–352, 2021.
- [8] Y. Lin, B. Chen, J. Wang, and Z. Bie, "A combined repair crew dispatch problem for resilient electric and natural gas system considering reconfiguration and dg islanding," *IEEE Transactions on Power Systems*, vol. 34, no. 4, pp. 2755–2767, 2019.
- [9] F. S. Gazijahani, J. Salehi, and M. Shafie-Khah, "A parallel fast-track service restoration strategy relying on sectionalized interdependent power-gas distribution systems," *IEEE Transactions on Industrial Informatics*, vol. 19, no. 3, pp. 2273–2283, 2022.
- [10] M. Z. Gargari, M. T. Hagh, and S. G. Zadeh, "Preventive scheduling of a multi-energy microgrid with mobile energy storage to enhance the resiliency of the system," *Energy*, vol. 263, p. 125597, 2023.
- [11] R. Hemmati, H. Mehrjerdi, and S. M. Nosratabadi, "Resilience-oriented adaptable microgrid formation in integrated electricity-gas system with deployment of multiple energy hubs," *Sustainable Cities and Society*, vol. 71, p. 102946, 2021.
- [12] M. Yan, Y. He, M. Shahidehpour, X. Ai, Z. Li, and J. Wen, "Coordinated regional-district operation of integrated energy systems for resilience enhancement in natural disasters," *IEEE Transactions on Smart Grid*, vol. 10, no. 5, pp. 4881–4892, 2018.
- [13] Z. Wang, T. Ding, W. Jia, C. Huang, C. Mu, M. Qu, M. Shahidehpour, Y. Yang, F. Blaabjerg, L. Li *et al.*, "Multi-stage stochastic programming for resilient integrated electricity and natural gas distribution systems against typhoon natural disaster attacks," *Renewable and Sustainable Energy Reviews*, vol. 159, p. 111784, 2022.
- [14] T. Chen, X. Xu, H. Wang, and Z. Yan, "Routing and scheduling of mobile energy storage system for electricity arbitrage based on two-layer deep reinforcement learning," *IEEE Transactions on Transportation Electrification*, vol. 9, no. 1, pp. 1087–1102, 2022.
- [15] M. Nazemi, P. Dehghanian, X. Lu, and C. Chen, "Uncertainty-aware deployment of mobile energy storage systems for distribution grid resilience," *IEEE Transactions on Smart Grid*, vol. 12, no. 4, pp. 3200–3214, 2021.
- [16] S. Ghasemi and J. Moshtagh, "Distribution system restoration after extreme events considering distributed generators and static energy storage systems with mobile energy storage systems dispatch in transportation systems," *Applied Energy*, vol. 310, p. 118507, 2022.
- [17] J. Kim and Y. Dvorkin, "Enhancing distribution system resilience with mobile energy storage and microgrids," *IEEE Transactions on Smart Grid*, vol. 10, no. 5, pp. 4996–5006, 2018.
- [18] S. Yao, P. Wang, X. Liu, H. Zhang, and T. Zhao, "Rolling optimization of mobile energy storage fleets for resilient service restoration," *IEEE Transactions on Smart Grid*, vol. 11, no. 2, pp. 1030–1043, 2019.
- [19] W. Shi, H. Liang, and M. Bittner, "Stochastic planning for power distribution system resilience enhancement against earthquakes considering mobile energy resources," *IEEE Transactions on Sustainable Energy*, 2023.
- [20] R. Alonso and A. Z. de Souza, "Resilience of active networks with optimal mobile energy storage systems management," *Electric Power Systems Research*, vol. 217, p. 109152, 2023.
- [21] Q. Shi, W. Liu, B. Zeng, H. Hui, and F. Li, "Enhancing distribution system resilience against extreme weather events: Concept review, algorithm summary, and future vision," *International Journal of Electrical Power & Energy Systems*, vol. 138, p. 107860, 2022.
- [22] D. K. Mishra, M. J. Ghadi, A. Azizivahed, L. Li, and J. Zhang, "A review on resilience studies in active distribution systems," *Renewable and Sustainable Energy Reviews*, vol. 135, p. 110201, 2021.
- [23] Q. Zhang, Z. Wang, S. Ma, and A. Arif, "Stochastic pre-event preparation for enhancing resilience of distribution systems," *Renewable and Sustainable Energy Reviews*, vol. 152, p. 111636, 2021.
- [24] A. Arif, Z. Wang, C. Chen, and B. Chen, "A stochastic multi-commodity logistic model for disaster preparation in distribution systems," *IEEE Transactions on Smart Grid*, vol. 11, no. 1, pp. 565–576, 2019.
- [25] F. S. Gazijahani, J. Salehi, and M. Shafie-khah, "Benefiting from energy-hub flexibilities to reinforce distribution system resilience: A pre-and post-disaster management model," *IEEE Systems Journal*, vol. 16, no. 2, pp. 3381–3390, 2022.
- [26] Y. Zeng, C. Qin, J. Liu, and X. Xu, "Coordinating multiple resources for enhancing distribution system resilience against extreme weather events considering multi-stage coupling," *International Journal of Electrical Power & Energy Systems*, vol. 138, p. 107901, 2022.
- [27] J. Christiansen, B. Dandurand, A. Eberhard, and F. Oliveira, "A study of progressive hedging for stochastic integer programming," *Computational Optimization and Applications*, pp. 1–46, 2023.
- [28] B. Taheri, A. Safdarian, M. Moeini-Aghtaie, and M. Lehtonen, "Distribution system resilience enhancement via mobile emergency generators," *IEEE Transactions on Power Delivery*, vol. 36, no. 4, pp. 2308–2319, 2020.
- [29] H. Gao, Y. Chen, S. Mei, S. Huang, and Y. Xu, "Resilience-oriented pre-hurricane resource allocation in distribution systems considering electric buses," *Proceedings of the IEEE*, vol. 105, no. 7, pp. 1214–1233, 2017.
- [30] X. Wang, Y. Tan, T. Zhang, R. Xiao, K. Yu, and J. Zhang, "Numerical study on the diffusion process of pinhole leakage of natural gas from underground pipelines to the soil," *Journal of Natural Gas Science and Engineering*, vol. 87, p. 103792, 2021.
- [31] B. Chen, J. Wang, X. Lu, C. Chen, and S. Zhao, "Networked microgrids for grid resilience, robustness, and efficiency: A review," *IEEE Transactions on Smart Grid*, vol. 12, no. 1, pp. 18–32, 2020.
- [32] Z. Ye, C. Chen, B. Chen, and K. Wu, "Resilient service restoration for unbalanced distribution systems with distributed energy resources by leveraging mobile generators," *IEEE Transactions on Industrial Informatics*, vol. 17, no. 2, pp. 1386–1396, 2020.
- [33] B. Chen, C. Chen, J. Wang, and K. L. Butler-Purry, "Sequential service restoration for unbalanced distribution systems and microgrids," *IEEE Transactions on Power Systems*, vol. 33, no. 2, pp. 1507–1520, 2017.
- [34] Y. Wang, Y. Xu, J. Li, J. He, and X. Wang, "On the radiality constraints for distribution system restoration and reconfiguration problems," *IEEE Transactions on Power Systems*, vol. 35, no. 4, pp. 3294–3296, 2020.
- [35] R. Xu, C. Zhang, D. Zhang, Z. Y. Dong, and C. Yip, "Adaptive robust load restoration via coordinating distribution network reconfiguration and mobile energy storage," *IEEE Transactions on Smart Grid*, 2024.

BIOGRAPHIES

